Proceedings of the ASME 2010 International Mechanical Engineering Congress & Exposition
IMECE2010
November 12-18, 2010, Vancouver, British Columbia, Canada

IMECE2010-40948

STRESS APPROXIMATION TECHNIQUE FOR HELICAL COMPRESSION SPRINGS SUBJECTED TO LATERAL LOADING

Scott G. Keller
University of Central Florida
Orlando, Florida, USA

Ali P. Gordon
University of Central Florida
Orlando, Florida, USA

ABSTRACT

Helical compression springs are commonly used devices capable of storing kinetic energy. Typical applications vary in simplicity, ranging from low stress amplitudes and in favorable environments, e.g. ball point pen spring at room temperature, to millions of cycles in elevated temperatures, e.g. valve train spring in IC engines. Regardless of the load or environment, springs are able to use the intrinsic elasticity of the material and the initial geometry to resist plastic deformation, all while allowing for the transfer of load over various distances. Generally, these loads are parallel to the axis of the spring; however, as more complex designs arise, these uniaxial springs are gaining popularity in a variety of off-axis loading situations, e.g. flexible shaft couplings, invalidating traditional stress/strain equations. As such, equivalent stress and strain equations have been developed capable of fast, real-time calculations based upon visual inspection of the bent helix. Coupled with the initial dimensions and material of the spring, the state of equivalent stress/strain can be resolved at any position within the wire. Experiments were conducted on several off-the-shelf steel springs (conforming to ASTM A229), then compared to FEA and analytical solutions. Ultimately, it was observed that through an approximation of the bent helix, the equivalent stress and strain can be determined at any location within the wire, allowing for the approximation of life and crack initiation locations of the spring.

NOMENCLATURE

α	Spring Helix Angle
ε_i	Strain in *i*-th Direction [in/in (mm/mm)]
ε_{vm}	Equivalent Strain [in/in (mm/mm)]
θ_T	Angular Deflection
ν	Poisson's Ratio
ρ	Radius of Curvature [in (mm)]
σ_i	Stress in *i*-th Direction [ksi (MPa)]
σ_{vm}	Equiavlent Stress [ksi (MPa)]
τ	Shear Stress [ksi (MPa)]
d	Wire Diameter [in (mm)]
y_{max}	Distance from Neutral Axis, max [in (mm)]
A	Cross Sectional Area [in^2 (mm^2)]
C	Spring Index
D	Spring Diameter [in (mm)]
E	Elastic Modulus [Msi (GPa)]
F	Externally Applied Force [lbf (N)]
G	Shear Modulus [Msi (GPa)]
GF	Gage Factor
I	Second Moment of Inertia [in^4 (mm^4)]
J	Polar Moment of Inertia [in^4 (mm^4)]
K_s	Shear Stress Correction Factor
K_w	Wahl Factor
L_0	Free Length [in (mm)]
M	Externally Applied Moment [lbf·in (N·mm)]
N_a	Number of Active Coils
ΔR	Change in Resistance [Ω]
R	Radius [in (mm)]
R_i	Initial Resistance [Ω]
T	Externally Applied Torque [lbf·in (N·mm)]
ΔV_{out}	Change in Voltage [V]
V_{ex}	Excitation Voltage [V]

INTRODUCTION

Helical compression springs have become commonplace in designs requiring the gradual application of load. Compressive forces are typically exerted aligned with the spring helix and applied concentrically with the coils, as is the case in automotive valve springs and suspension components. Spring designers tailor the shape and size of axial compression springs to meet the design requirements without accounting for non-negligible off-axis or multiaxial loading [1]; however, as more complex designs incorporate larger degrees of multiaxial load carrying capability, the effects of uniform and non-uniform bending must be considered.

The shear stress formulation commonly found in engineering texts has gained notoriety as being the dominate stress throughout the coils [2,3]. Summarized in texts in the 1960s [4], the state of stress can be related to the externally applied force and the physical properties of the spring, i.e.,

$$\tau = \frac{F}{A} + \frac{TR}{J} \tag{1}$$

where the first term accounts for direct shear and the second is the shear stress due to torsion. Additional simplification furnishes the shears stress as a function of F, D and d, i.e.,

$$\tau = \frac{4F}{\pi d^2} + \frac{8FD}{\pi d^3}. \tag{2}$$

Through the use of a shear stress correction factor, K_s, Eq. (2) can be further reduced, e.g.,

$$\tau = K_s \frac{8FD}{\pi d^3}. \tag{3}$$

The shear stress correction factor, K_s, accounts for the increase or decrease in stress based on the location on the wire that is under observation. Achieving more accuracy, the Wahl Factor, K_w, has been used to replace K_s, which solely depends on the spring index, C, i.e.,

$$K_w = \frac{4C-1}{4C-4} + \frac{0.615}{C}. \tag{4}$$

Substitution of Eq. (4) into Eq. (3) furnishes the maximum shear stress, which occurs along the inside of the coil due to the curvature effect, i.e.,

$$\tau_{max} = K_w \frac{8FD}{\pi d^3}; \tag{5}$$

however, this maximum shear stress and its location are the result of an axially applied load, with no consideration given to off spring-axis or eccentric loads. The location of maximum stress remains constant, regardless of the magnitude of load applied.

Equally important in design considerations, the axial deflection experienced upon the application of load can be equated through the use of Castigliano's theorem, under the assumption that the spring is elastic, homogenous, isotropic and has uniform dimensions, e.g.,

$$\delta = \frac{8FD^3 N_a}{d^4 G}\left(1 + \frac{1}{2C^2}\right). \tag{6}$$

The latter term in parenthesis in Eq. (6) essentially reduces to unity, allowing for the simplification with a small assumption. Generally, in design calculations, Eqs. (5) and (6) are regarded as the governing stress and deflection models for uniaxially loaded springs [3-5]. Thus, torsion dominates the stress distributed on the helixes cross-section, validating the reduction of Eq. (1).

To properly account for the bending stresses that are encountered during multiaxial loading, elementary beam theory provides for the maximum stress encountered in a cantilever beam as a function of the bending moment [6], i.e.,

$$\sigma_{max} = \frac{My_{max}}{I}. \tag{7}$$

Figure 1: *Standard helical compression spring subjected to a uniaxial load along the central axis of the helix.*

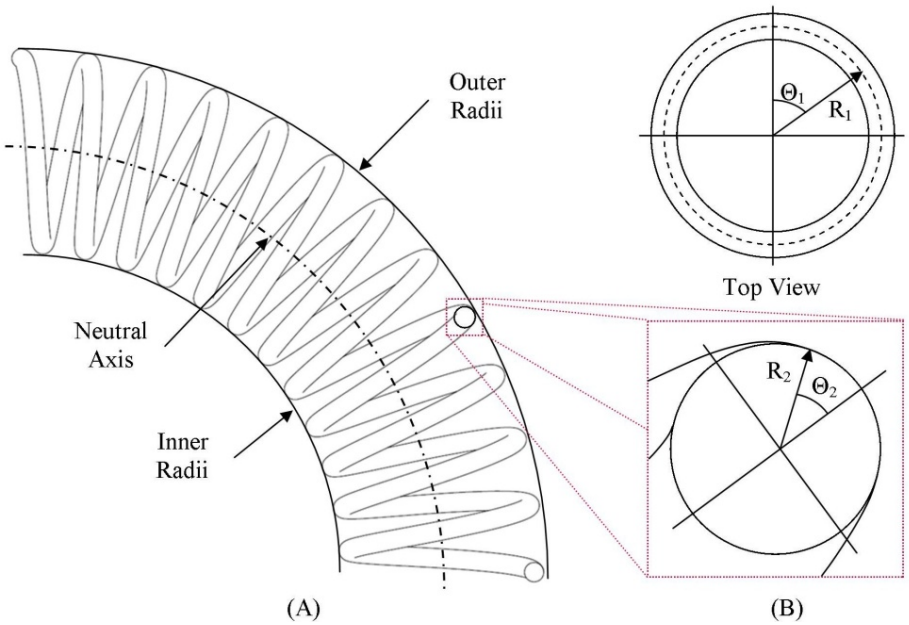

Figure 2: *View of deformed helical compression spring subjected to a uniform moment, with location of the specified helix and coil reference frames.*

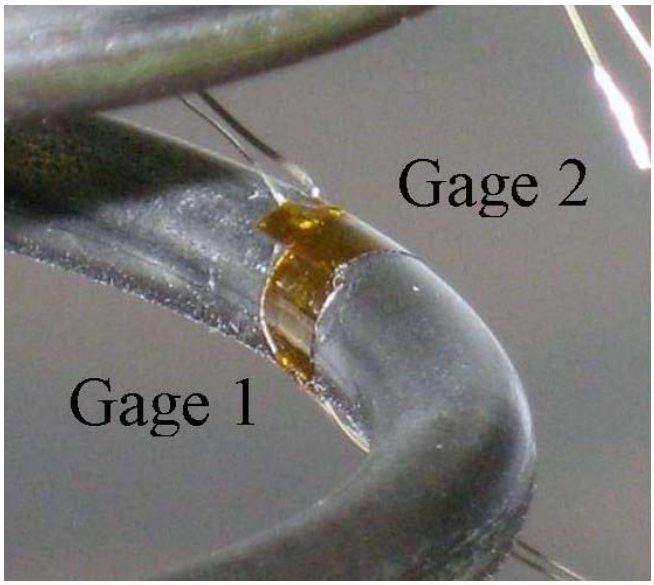

Figure 3: *Strain gages 1 and 2 affixed to the subject steel compression spring used in this study (3 and 4 are 180° opposite).*

Equation (7) will be utilized further in developing the stress formulation at any location in the next section.

A limitation to existing analytical models of stress distributions in springs is that they require that either the externally applied force, F, or the applied moment, M, is known. In the case of flexible shaft couplings, however, these forces and moments can be difficult to calculate if the curvature is variable. That is to say, the nature of the spring lends itself to being able to infer deflection from inspection rather than load. Ability to measure deflection with relative ease compared to load provokes the necessity for a deflection-based method of stress determination.

BENDING ANALYSIS

Previous works suggest that when a spring undergoes bending, the wire is subjected to both torsion and flexure [7,8]. Wolansky has studied the effects of bending on helical compression springs and formulated expressions for both flexural and torsional stresses experienced, i.e.,

$$\sigma = \frac{16M}{\pi d^3} \quad \text{and} \quad \tau = \frac{8M}{\pi d^3}. \tag{8}$$

Under the application of a pure moment, the angular deflection, θ_T, can be approximated as a function of the applied moment and material properties [8,9], i.e.,

$$\theta_T = \frac{32MN_a(2+\nu)D}{d^4E}. \tag{9}$$

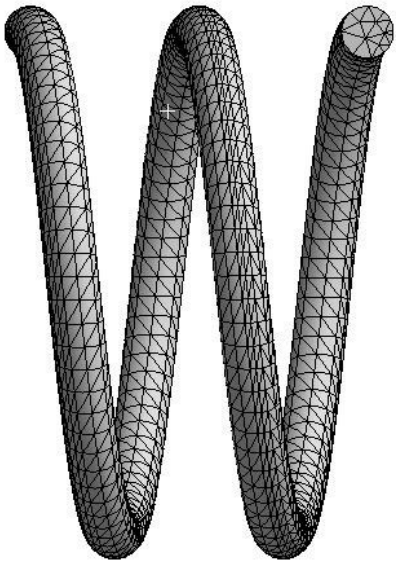

Figure 4: *Extracted coils used in the numerical simulation.*

It is assumed that a helical compression spring subjected to uniaxial loading through the central axis only, Fig. 1, enabling the use of Eqs. (5) and (6). However, when a moment is applied to the ends, as in Fig. 2, stresses due to bending must be accounted for. Positions along the spring are shown using R_1, R_2, θ_1 and θ_2, where R_1 is distance to the center of the wire, θ_1 is the angle made with respect to a defined axis, R_2 is the distance from the center of the wire and θ_2 is the angle made with respect to a defined axis in the wire.

Upon observation, the wire is expected to exhibit a torsional state of stress at cross-sections along the inner and outer radius, while a bending state of stress is expected along the neutral axis. Using the defined coordinate system, both the torsional and bending stresses can be resolved into individual components, i.e.,

$$\tau = K_w \frac{TR_2}{J}\cos\theta_1 \tag{10}$$

$$\sigma = \frac{MR_2}{I}\sin\theta_1 \sin\theta_2 \tag{11}$$

As θ_1 rotates from 0 to $\pi/2$ (from the outer/inner radius to the neutral axis), the state of stress is expected to transform from pure torsion to pure bending. By equilibrium conditions, the torque, T, and the moment, M, are equivalent and Eqs. (10) and (11) can be combined to form a single, scalar-valued quantity using the von Mises equivalent stress formulation, i.e.,

$$\sigma_{vm} = \frac{TR_2}{J}\sqrt{4\sin^2\theta_1 \sin^2\theta_2 + 3K_w{}^2\cos^2\theta_1}. \tag{12}$$

Additionally, the torque can be approximated through visual inspection of the bent helix. With knowledge of the free

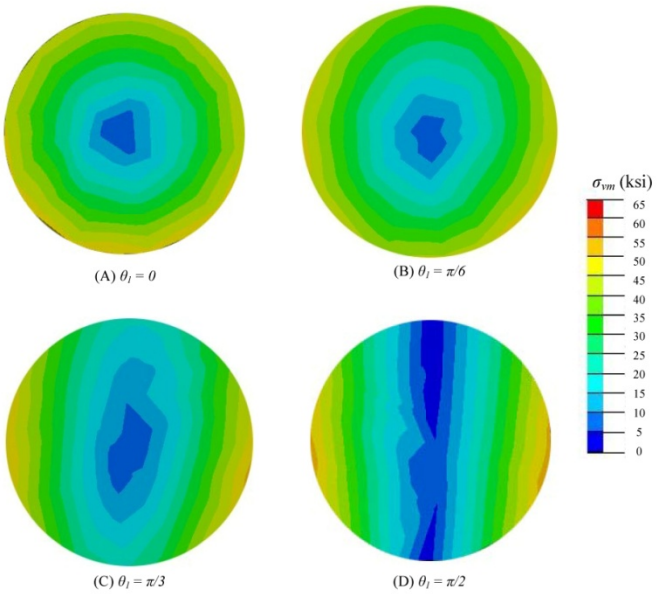

Figure 5: *Extracted coil from the full model, revealing the transition from a torsional state of stress (A) to a bending state of stress (D) and the intermediary stress distributions (B and C).*

length of the spring and the radius of curvature, the torque can be approximated,

$$T = \frac{d^4 G L_0}{32 D N_a \rho}. \tag{13}$$

Combining Eqs. (12) and (13), the equivalent stress at any point within the wire can be approximated, i.e.,

$$\sigma_{vm} = \frac{d^4 G L_0}{32 D N_a \rho} \cdot \frac{R_2}{J}\sqrt{4\sin^2\theta_1 \sin^2\theta_2 + 3K_W{}^2 \cos^2\theta_1}. \tag{14}$$

Equation (14) can be used to approximate the equivalent stress at any position within the wire based solely upon visual inspection of the bent helix. It should noted that the spring is expected to be a linear, elastic material with a uniform, symmetric cross section and the load imposed does not induce yielding of the material. If these conditions are not met, Eq. (14) is no longer valid and additional measures must be taken to properly determine the state of stress.

EXPERIMENTAL AND NUMERICAL ANALYSIS

To characterize the states of both stress and strain under mechanical loading, springs (or their numerical renderings) are often subject to loading at their ends and the deflection is analyzed [9]. For the experimental portion of the current study, a generic compression spring was selected and subjected to an end moment. The dimensions (Table 1) and properties (Table 2) of the subject spring for this study were selected for several

Table 1 - Spring Geometric Properties

Wire Diameter, d [in (mm)]	0.20
Mean Diameter, D [in (mm)]	1.98
Free Length, L_0 [in (mm)]	8.00
Solid Length, L_s [in (mm)]	2.59
Number of Active Coils, N_a	10.5
Spring Index, $C = D/d$	9.57
Spring Rate, k [lb/in (N/mm)]	32.3
End Conditions	Closed and Ground

Table 2 - Spring Material

Elastic Modulus, E [Msi (GPa)]	30.0 (207)
Shear Modulus , G [Msi (GPa)]	11.5 (79.3)
Yield Strength, S_y [ksi (MPa)]	>115 (>795)*
Ultimate Strength, S_{ut} [ksi (MPa)]	229.5 (1580)*
Poisson's Ratio, v	0.292

*Value is proprietary to spring maker; approximation

reasons. The spring was designed to be large enough to be equipped with typical foil strain gages. The wire material was selected to A229, a commonly used standard for spring material.

Both N_a and C were designed to be well within their recommended ranges for static service [4], i.e.,

$$3 \le N_a \le 15, \tag{15}$$

$$4 \le C \le 12. \tag{16}$$

Based on both the mechanical properties and the dimensions, a spring rate [e.g. F/δ from Eq. (6)] of 32.3 lb/in (5.7 kN/m) results. This spring design confers a low enough stiffness for the spring to be loaded manually and a large enough stiffness to be mechanically loaded by a tabletop universal test frame. An additional limitation that is imposed is that of the helix angle and the spring index. Equations (15) and (16) are valid whenever α is less than 15° and C is greater than 3.7 [2]. For most practical purposes, these conditions are met for flexible shaft couplings, as more coils and smaller helix angles provide stability. In the event large pitch angles are used, these effects must be taken into account.

Experiments were carried out on readily available, off-the-shelf helical compression springs that conform to ASTM A229. Specifically, the springs were Class II, having a strength requirement of 216 ksi (1489 MPa). The physical dimensions of the spring, as well as the high strength, allowed for the attachment of strain gages at various locations along the helix.

Linear strain gages were affixed to the surface of the spring at locations of expected maximum strain, Fig. 3. With the

experimental rig developed to impose pure bending, the spring was able to rotate so that the gages can be placed along the neutral axis or the inner/outer radius. Under the application of a lateral load, these gages can capture the strains at the key locations to determine the state of strain [13].

To compare the equivalent stress experienced and that predicted by Eq. (14), an equivalent strain formulation is needed. The equivalent von Mises strain, Eq. (17), could then be reduced to include only one axial strain, Eq. (18), i.e.,

$$\varepsilon_{vm} = \frac{1}{1+\nu} \cdot \sqrt{\frac{\left(\varepsilon_x - \varepsilon_y\right)^2 + \left(\varepsilon_y - \varepsilon_z\right)^2 + \left(\varepsilon_z - \varepsilon_x\right)^2 - 6\left(\gamma_{xy}{}^2 + \gamma_{yz}{}^2 + \gamma_{zx}{}^2\right)}{2}} \quad , \tag{17}$$

$$\varepsilon_{vm} = \frac{1}{1+\nu} \cdot \varepsilon_x \quad . \tag{18}$$

Rearranging the gage factor equation, Eq. (19), the uniaxial strain can be obtained through a change in the resistance of the strain gage, e.g.,

$$\varepsilon_x = \frac{\Delta R / R_i}{GF} \quad . \tag{19}$$

where ΔR is the change in resistance of the strain gage, R is the initial strain gage resistance and $G.F.$ is the gage factor of the strain gage. Furthermore, in a quarter Wheatstone bridge, when the change in resistance of the strain gage is significantly less than the initial resistance, the change in resistance can be related to the change in voltage, Eq. (20) [14],

$$\frac{\Delta R}{R_i} = \frac{4\Delta V_{out}}{V_{ex}} \quad , \tag{20}$$

where V_{out} is measured output voltage across the completed Wheatstone Bridge and V_{ex} is the excitation voltage used. Combining Eqs. (18), (19) and (20), the equivalent von Mises strain can be obtained through observation of the outputted voltage from quarter Wheatstone bridge when a uniaxial strain is imposed, i.e.,

$$\varepsilon_{vm} = \frac{1}{GF} \cdot \frac{1}{1+\nu} \cdot \frac{4\Delta V_{out}}{V_{ex}} \quad . \tag{21}$$

Equation (21) is valid whenever a uniaxial strain is applied to a linear, elastic and isotropic material.

Recently, analyses have been carried out on springs that involve the implementation of numerical routines. Many studies focused on the life-prediction of compression springs subjected to axial and multiaxial loading [9-12]. Particularly, numerical results were compared to existing analytical models

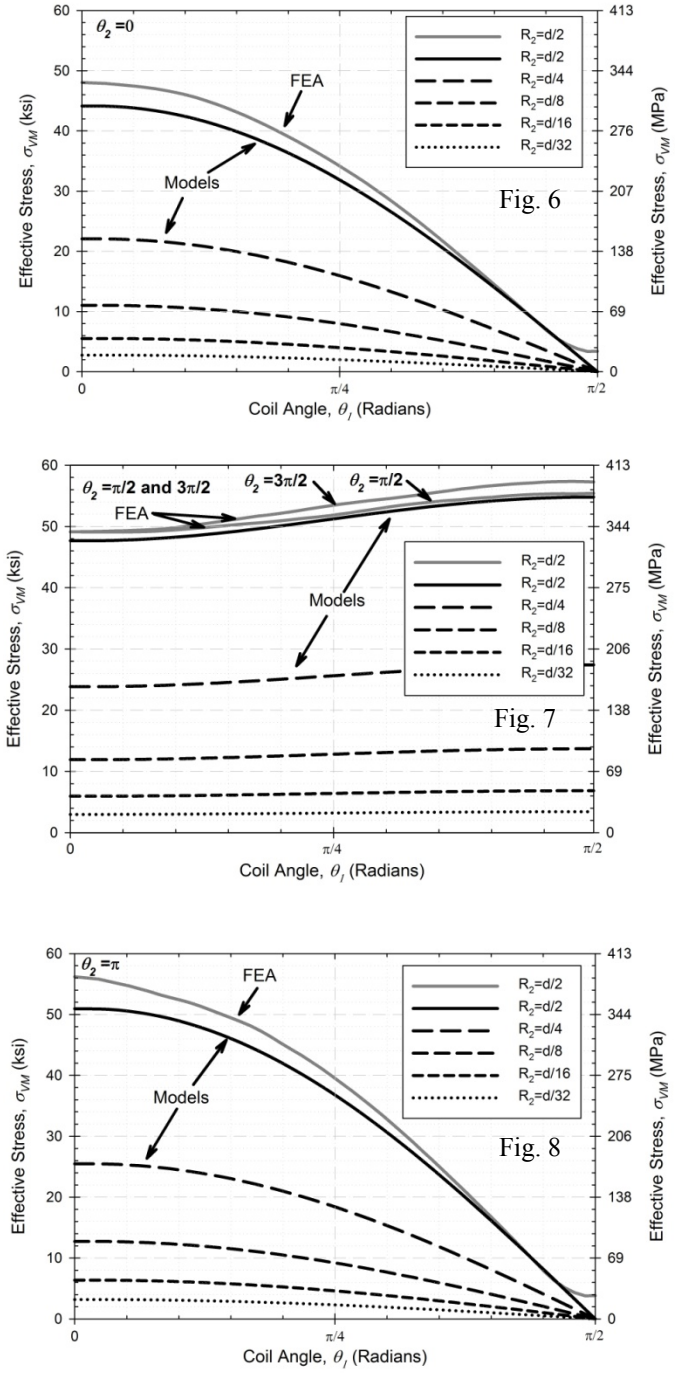

Figures 6-8: *Equivalent stress trajectories along (top) $\theta_2 = 0$ (middle) $\theta_2 = \pi/2$ and $\theta_2 = 3\pi/2$ and (bottom) $\theta_2 = \pi$ as θ_1 increases from 0 to $\pi/2$. Included are the actual and predicted maximum stresses, along with the predicted stresses at different distances from the wire neutral axis.*

that employ the critical plane approaches to predict multiaxial crack initiation [12]. Results published in the literature review provided strong correlation between analytical and numerical models.

Experimental and analytical solutions were compared to results from a finite element analysis (FEA). The spring used in the apparatus was rendered and a mesh of elements was created in ANSYS multipurpose software. The output from the numerical simulation provided the stresses as equivalent stresses (von Mises), as well as directional uniaxial stresses and strains; therefore, direct comparison between the predicted and actual stresses could be made.

To obtain a high fidelity resolution of the stress distribution, two coils were extracted from the full model and simulated as an independent submodel, Fig. 4. These coils were meshed utilizing quadratic tetrahedral elements with nodes that were unconstrained in all degrees of freedom. A total of 6,825 linear, 20-noded elements were contained in the model. Proportional displacements and conditions were applied to this submodel, resulting in identical stresses as the full model. From this submodel, effective stress trajectories were extracted for comparison with Eq. (14).

RESULTS AND DISCUSSION

Results from the numerical analysis were compared with values obtained from the experimental and analytical portions of this investigation. As expected, the spring underwent a change from a torsional state of stress to a bending state as θ_1 increased from 0 to $\pi/2$, i.e., from the inner/outer radius to the neutral axis. A single, half coil was extracted from the middle of the full model and the evolution of the stress field is shown, Fig. 5.

Upon further analyzing Fig. 5, several observations are made. Along the $\theta_1 = 0$ and π planes, a purely torsional state of stress is observed, Fig. 5A. A gradual change in the state of stress is seen at intermediate planes of $\theta_1 = \pi/6$ and $\theta_1 = \pi/3$, Figs. 5B and 5C, respectively. The change in the state of stress is completed once $\theta_1 = \pi/2$ and a cross-sectional slice at this position reveals a pure bending state of stress, Fig. 5D. This confirms the assumption that the stress distribution at any cross-section is a function based upon the distance from the neutral axis. Furthermore, it confirms that when multiaxial deflections are imposed onto helical compression springs, the stress distribution is not constant throughout the helix.

The non-uniform stress distribution is further emphasized through the mechanical tests conducted. As the gages rotate through $\theta_1 = 0$ to $\pi/2$, large changes in strains are observed, Table 3. With gages 1 and 3 located along the outer radii under multiaxial loading (location of pure torsion), strains are observed to deviate from both the strains predicted through Eq. (16) and those reported by FEA. As expected, the strain gage located inside the coil reported the largest strain, which can be attributed to the curvature of the wire. It is suggested that the linear strain gages may not be best suited to measure the state of strain at this location or that they are not affixed in an optimum orientation.

Unlike the strains reported by gages 1 and 3, large changes in strains are observed in gages 2 and 4 as θ_1 rotates from 0 to $\pi/2$. When these gages are located along the neutral axis, maximum bending stresses are observed, as indicated by the large strains. These results are in agreement with those from FEA and Eq. (14), as the three methods report similar results, Table 3. While these gages are orientated along the neutral axis, the strains reported are higher than any other predicted or observed strains, suggesting that bending stresses possibly outweigh torsional stresses.

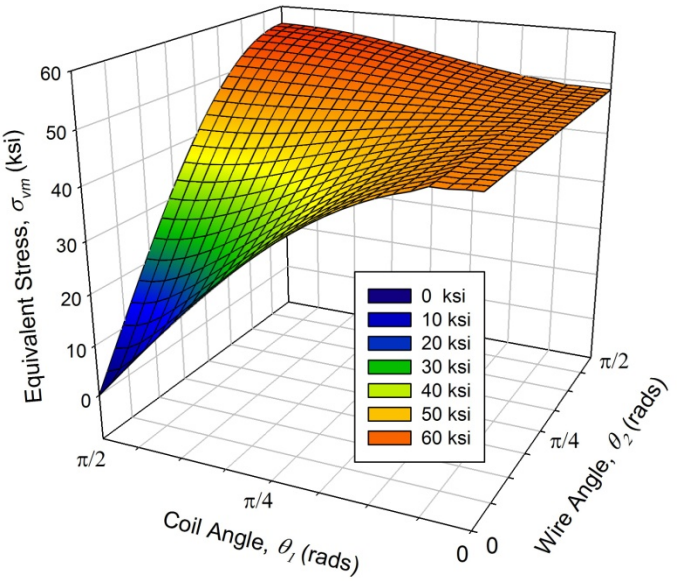

Figure 9: *Equivalent stresses along one representative, quarter turn of both θ_1 and θ_2, revealing the shift from pure shear to pure bending states of stress.*

Effective stress distributions along four key trajectories were extracted from the FEA model: on the outside (Fig. 6), top and bottom (Fig. 7), and inside (Fig. 8) of the coil at cross-sections ranging from $\theta_1 = 0$ to $\pi/2$. Each effective stress trajectory is compared to the predicted effective stress for that trajectory. Since each curve is cyclic in nature, only the distribution from $\theta_1 = 0$ to $\pi/2$ is included without loss of generality.

Table 3– Comparison of multiaxial effective strains, μin/in

	Exp	FEA	Eq.14
Gages along outer radii – π /2 Bend			
Gage 1 – ($R= d/2$, $\theta_1= 0$, $\theta_2= \pi$)	311.2	1873	1698
Gage 2 – ($R= d/2$, $\theta_1= 0$, $\theta_2= 3\pi/2$)	207.4	1637	1589
Gage 3 – ($R= d/2$, $\theta_1= 0$, $\theta_2= 0$)	233.4	1602	1471
Gage 4 – ($R= d/2$, $\theta_1= 0$, $\theta_2= \pi/2$)	155.6	1637	1589
Gages along neutral axis – π /2 Bend			
Gage 1 – ($R= d/2$, $\theta_1= \pi/2$, $\theta_2= \pi$)	77.8	126.6	53.3
Gage 2 – ($R= d/2$, $\theta_1= \pi/2$, $\theta_2= 3\pi/2$)	1901	1845	1827
Gage 3 – ($R= d/2$, $\theta_1= \pi/2$, $\theta_2= 0$)	77.8	112.4	46.2
Gage 4 – ($R= d/2$, $\theta_1= \pi/2$, $\theta_2= \pi/2$)	1919	1911	1827

The prediction of stresses at any location through the use of Eq. (14) is also shown in Figs. 6-8. Through visual inspection of the bent helix alone, equivalent stresses are approximated within 10% of their actual value with $R_2 = d/2$. Equation (14) is also capable of predicting the equivalent stress at any position on a cross-section, allowing for the reproduction the stress distribution throughout the wire. Additionally, through one quarter turn of both θ_1 and θ_2, a contour of the stresses experienced is provided, Fig. 9.

CONCLUSIONS

Based upon the observations of mechanical experiments and numerical simulations, an equivalent stress approximation technique for helical compression springs subjected to lateral loading is proposed. Through the approximation of the curvature of radius, coupled with the geometry and material properties, the equivalent stress at any location within the wire can be approximated. Crack initiation locations can be predicted by locating regions of the largest stress. Additionally, life predictions can be made with relative ease, as the state of a stress is easily resolved. Ultimately, a few "back-of-the-envelope" calculations can provide insight to the life of a helical compression spring subjected to lateral loading. Future work will continue on the stress approximation in springs subjected to non-uniform lateral loading, as well as a non-circular cross-sections.

REFERENCES

[1] Imaizumi, T., et al., *Shape Optimization of the Wire Cross Section of Helical Springs (Study on shapes of inner and outer boundaries of Wire with a Hole)*, Japan Society of Mechanical Engineers (JSME) International Journal, Volume 36 (4), pp. 507-514, 1993.

[2] Budynas, R., Nisbett, J. *Shigley's Mechanical Engineering Design* 8th Ed. New York: McGraw-Hill, 2008.

[3] Norton, R.L., *Machine Design – An Integrated Approach* 3rd Ed. New Jersey: Pearson Prentice Hall, 2006.

[4] Wahl, A.M., *Mechanical springs*, New York: McGraw-Hill, 1963.

[5] Carlson, H., *Spring Designer's Handbook*, New York: M. Dekker, 1978.

[6] Gould, P.L. *Introduction to Linear Elasticity* 2nd Ed. New York: Springer, New York, Inc, 1994

[7] Wolansky, E.B., *Bending of Helical Springs*, Springs, Volume 39 (2), pp. 76-80, 2000.

[8] Wolansky, E.B., *Conical Spring Buckling Deflection*, Springs, Volume 35 (1), pp. 62-68, 1996.

[9] Fakhreddine, D., et al., *Finite Element Method for the Stress Analysis of Isotropic Cylindrical Helical Spring*, European Journal of Mechanics A/Solids, Volume 24, pp. 1068–1078, 2005.

[10] Cook, R.D., *Finite Element Model of Closely-Coiled Helical Springs*, Computers and Structures, Volume 34 (1), pp. 179-180, 1990.

[11] Jiang, W.G., Henshall, J.L., *A Novel Finite Element Model for Helical Springs*, Finite Elements in Analysis and Design, Volume 35, pp. 363-377, 2000.

[12] Del Llano-Vizcaya, L., et al., *Multiaxial fatigue and failure analysis of helical compression springs*, Engineering Failure Analysis, Volume 13, pp. 1303–1313, 2006.

[13] *How Strain Gages Work*, KYOWA Sensor System Solutions, Japan, Undated Handout.

[14] Figliola, R.S., Beasley, D.E., *Theory and Design for Mechanical Measurements*, 3rd Ed., New Jersey: John Wiley and Sons, Inc., 2000.